


# Scalable production of hydrophobic starch/beeswax films by continuous solution casting

Bruno Ribeiro Luchesi<sup>1,2</sup>  | Francys Kley Vieira Moreira<sup>2,3</sup> | José Manoel Marconcini<sup>1,2</sup>

<sup>1</sup>Nanotechnology National Laboratory for Agriculture (LNNA), Embrapa Instrumentação, Rua XV de Novembro, São Paulo, Brazil

<sup>2</sup>Graduate Program in Materials Science and Engineering, Federal University of São Carlos, Rodovia Washington Luis, São Paulo, Brazil

<sup>3</sup>Materials Engineering Department, Federal University of São Carlos, Rodovia Washington Luis, São Paulo, Brazil

## Correspondence

Bruno Ribeiro Luchesi, Nanotechnology National Laboratory for Agriculture (LNNA), Embrapa Instrumentação, Rua XV de Novembro, 1452, São Carlos, São Paulo 13560-970, Brazil.

Email: [luchesi.bruno@gmail.com](mailto:luchesi.bruno@gmail.com)

## Funding information

Coordenação de Aperfeiçoamento de Pessoal de Nível Superior, Grant/Award Number: 88887.388245/2019-00

## Abstract

Starch is an appealing natural polymer for the scaled-up production of biodegradable plastics. However, the low water resistance of starch has made its broad applicability largely doubted. In this study, starch was combined with beeswax (BW) through a pilot scale continuous solution casting (CSC) technique to reduce water affinity while keeping the ensuing films totally biodegradable. The phase morphology, surface wettability, and water vapor permeability (WVP) of films were examined over a broad BW–starch mass ratio (0.3–0.7). Emulsified, surfactant-free starch/BW films were successfully obtained at a productivity of 0.55 m<sup>2</sup> film h<sup>-1</sup>. The water contact angle increased nearly by 100% at 30 wt% BW, leading to remarkable reductions in WVP. BW droplets well distributed within the starch matrix played a key role in enhancing the water barrier properties of films. CSC of starch/BW films offers a basis to design new hydrophobic formulations for applications that require biodegradable plastics with high moisture resistance.

## KEYWORDS

beeswax, continuous solution casting, scalable production, starch, water vapor permeation

## 1 | INTRODUCTION

Plastic films based on nonbiodegradable polymers require decades to deteriorate in the environment and, therefore, create several negative environmental impacts when disposed in an improper way.<sup>1</sup> In this context, starch has been extensively researched for the development of biodegradable films over the last decades.<sup>2–4</sup> Starch is the main plant-derived energy source that is composed of two carbohydrate polymers: amylose, built almost linearly by glucose units connected by  $\alpha$ -(1→4) glycosidic linkages, and amylopectin, which structurally differs from amylose due to long ramifications featured by  $\alpha$ -(1→6) glycosidic linkages as branching points every 22–70 glucose units.<sup>5,6</sup>

Starch gelatinization is a primary step for biodegradable film production, but it exposes the hydroxyl groups of starch polymers, increasing the hydrophilic character of the ensuing films. Polar plasticizers are also required in the process to achieve a starch film mechanically viable, but they make the films even more hydrophilic. Therefore, compounding or coating starch with hydrophobic agents have been attempted as feasible solutions for producing biodegradable films less susceptible to moisture for an extended range of applications.<sup>7–11</sup>

Beeswax (BW) has emerged as an eligible hydrophobic agent for the development of starch films with satisfactory levels of hydrophobicity. BW is a complex mixture of about 300 low-polarity substances, mostly esters (67 wt%), hydrocarbons (14 wt%), and fatty acids

(12 wt%).<sup>12</sup> The main advantages of BW as a component of starch films include its natural, biodegradable, and nontoxic features, in addition to being cheap, abundant, and easy to handle.<sup>13–15</sup>

BW has been used as a hydrophobic agent in starch films, including chemically and/or physically modified starches, achieving substantially lower water vapor permeability (WVP) and surface wettability.<sup>15–17</sup> However, most of these achievements involved the use of low BW contents and its stabilization with surfactants, and the films were produced by bench solution casting, a small-scale technique usually employed to obtain modified starch films.<sup>2,18–21</sup> Bench casting fails in achieving high film productivity due to the relatively long drying times (e.g., 12–24 h), which may be unsuited for starch/BW solutions, as the fast BW solidification induces phase separation in the ensuing films if no surfactant is used. In this context, continuous solution casting (CSC) appears as a suitable processing technique for obtaining BW-modified hydrophobic starch films. Recent studies demonstrated that CSC is highly effective in speeding up the processing of bio-based aqueous formulations, attaining films with good physical properties for food packaging applications.<sup>22,23</sup> Continuous casting of starch/BW solutions, however, has not been explored in the literature yet.

Hence, this work was aimed at modifying the interactions of starch films with water by incorporating BW through CSC. It is hypothesized here is that high speed of the CSC process may overcome the fast solidification of BW, enhancing its homogenization with starch, thereby leading to biodegradable films with superior moisture barrier properties. To prove this hypothesis, starch solutions covering a broad range of BW contents (30–70 wt%) were processed by CSC with no use of surfactants. The optical, WVP and surface wettability of the starch/BW films were determined to provide evidence of the CSC effectiveness.

## 2 | MATERIALS AND METHODS

### 2.1 | Materials

Regular corn starch (CS) (72 wt% amylopectin and 28 wt% amylose) was supplied by Ingredion (São Paulo, Brazil). High-purity BW ( $\rho = 0.826 \text{ g cm}^{-3}$ ,  $T_m = 64^\circ\text{C}$ ) was purchased from Wendel & Mecca Produtos Naturais (São Carlos, Brazil). Glycerol (99.5%) was supplied by Dinâmica Contemporânea LTDA (Diadema, Brazil). Deionized water ( $\rho = 18.2 \text{ M}\Omega \text{ cm}$ ) was obtained from a Milli-Q system (Barnstead Nanopure Diamond, Thermo Fisher Scientific Inc., Marietta, USA).

### 2.2 | Preparation of CS/BW filmogenic solutions

CS was dispersed manually at 7 wt% in deionized water previously mixed with glycerol at room temperature. The mixture was heated at  $80^\circ\text{C}$  in an oil bath under mechanical stirring for 30 min to complete the starch gelatinization. To obtain the filmogenic starch/BW solutions, solid BW was added to the gelatinized starch solution at  $80^\circ\text{C}$  under prolonged mechanical stirring for 5 min, until a completely homogenized solution was formed. The BW content was varied in 0, 30, 50, and 70 wt%, while the glycerol content was fixed at 30 wt%, both on a dry starch mass basis. All solutions were equilibrated at  $65^\circ\text{C}$  to be immediately used in the continuous casting process.

### 2.3 | Continuous solution casting

The CS/BW films were obtained by CSC in a KTF-B equipment (Mathis, Switzerland). The overall process is illustrated in Figure 1. In brief, the freshly prepared solution was initially poured onto a BoPET substrate (Mylar<sup>®</sup>) moving at constant speed ( $v = 0.12 \text{ m min}^{-1}$ ). The solution was immediately carried through a coating device equipped with a stationary doctor blade, forming a wet solution layer onto the substrate (Figure 1a). The wet layer thickness was controlled at 1.3 mm by adjusting the substrate to the blade gap with a dial indicator pair ( $\pm 0.001 \text{ mm}$ ). The wet solution layer was continuously moved through an infrared pre-drying chamber at  $65^\circ\text{C}$  and two air-circulating ovens (E1 and E2) at 80 and  $120^\circ\text{C}$  (Figure 1b), respectively, forming a dried film in the second oven outlet that was coiled (Figure 1c) and stored for further characterizations.

Four different films were produced according to the procedure described above. The film without BW (control film) was denominated as CS, while those with BW were denominated as 10/XBW, that is, X g of BW ( $X = 3, 5, \text{ or } 7 \text{ g}$ ) to 10 g of starch. The composition, BW volumetric fraction ( $\phi_{\text{BW}}$ ), thickness, and moisture content of the films are provided in Table 1.

### 2.4 | Characterizations

#### 2.4.1 | Differential scanning calorimetry

Differential scanning calorimetry (DSC) curves were recorded on a Q2000 calorimeter (TA Instruments) using dynamic  $\text{N}_2$  atmosphere flowing at  $50 \text{ mL min}^{-1}$  and sample sizes of 30–40 mg placed in open aluminum pans. The DSC analyses were carried out to simulate the

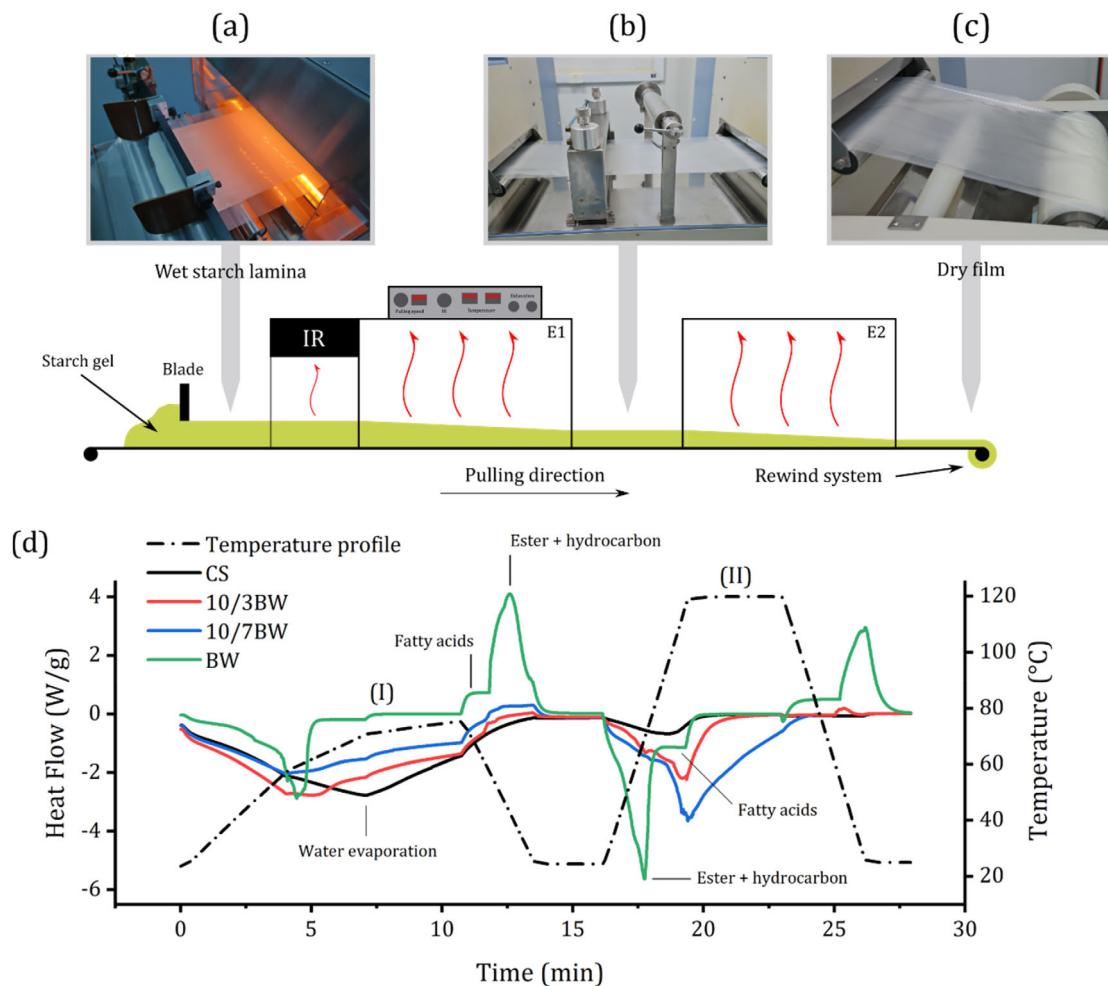


**FIGURE 1** Schematic flowchart of the continuous solution casting process: (a) wet layer formation, (b) outcome of wet layer passage through air circulating ovens, and (c) collection at the oven outlet—aligned with (d) differential scanning calorimetry curves (heat flow vs. time) of pure starch (CS), 10/3BW and 10/7BW starch/BW solutions, and pure BW (below). The dash line represents the temperature profile regarding the KTF-B equipment (heating zone I—IR pre-dryer + first air-circulating oven with  $T_{\max} = 80^{\circ}\text{C}$ ; heating zone II—second air-circulating oven with  $T = 120^{\circ}\text{C}$ ). BW, beeswax; CS, corn starch. [Color figure can be viewed at [wileyonlinelibrary.com](https://onlinelibrary.wiley.com/doi/10.1002/app.54730)] [wileyonlinelibrary.com](https://onlinelibrary.wiley.com/doi/10.1002/app.54730)]

**TABLE 1** Description of corn starch (CS)/beeswax (BW) films produced by continuous solution casting.

Sample	BW (wt%) <sup>a</sup>	BW (vol%) <sup>b</sup>	Glycerol (wt%) <sup>a</sup>	Thickness ( $\mu\text{m}$ ) <sup>c</sup>	Moisture (wt%) <sup>a</sup>
CS	0	0.00	30	$44 \pm 4^{\text{d}}$	$3.61 \pm 0.06^{\text{d}}$
10/3BW	30	0.27	30	$61 \pm 5^{\text{d}}$	$3.38 \pm 0.19^{\text{d}}$
10/5BW	50	0.38	30	$47 \pm 2^{\text{d}}$	$3.20 \pm 0.06^{\text{d}}$
10/7BW	70	0.46	30	$46 \pm 5^{\text{d}}$	$3.12 \pm 0.08^{\text{d}}$

<sup>a</sup>wt/wt of dry starch mass.

<sup>b</sup>BW volumetric fraction ( $\phi_{\text{BW}}$ ).

<sup>c</sup>Average film thickness ( $n = 3$ ) determined with a digital micrometer (Mitutoyo Manufacturing, Japan).

<sup>d</sup>Confidence level of statistical analysis was 95% ( $p < 0.05$ ).

thermal cycles to which the solutions are subjected to the continuous casting process as follows: first heating scan to  $65^{\circ}\text{C}$  at  $20^{\circ}\text{C min}^{-1}$  and then to  $80^{\circ}\text{C}$  at  $5^{\circ}\text{C min}^{-1}$  (relative to the IR pre-dryer stage); isotherm at  $80^{\circ}\text{C}$  for about 4 min (relative to the first oven); first

cooling scan down to  $25^{\circ}\text{C}$  at  $20^{\circ}\text{C min}^{-1}$ ; second isotherm at  $25^{\circ}\text{C}$  for about 3 min (relative to the gap between ovens); second heating scan up to  $120^{\circ}\text{C}$  at  $30^{\circ}\text{C min}^{-1}$ ; isotherm at  $120^{\circ}\text{C}$  for about 4 min (relative to the second oven); second cooling scan down to  $25^{\circ}\text{C}$

at 30°C min<sup>-1</sup>; and finally isotherm at 25°C for 2 min. The DSC analyses were performed with one repetition per sample.

## 2.4.2 | X-ray diffraction

The x-ray diffraction (XRD) patterns of samples were recorded with a Lab X-XRD 6000 equipment (Shimadzu) operating with CuK<sub>α</sub> radiation ( $\lambda = 1.5405 \text{ \AA}$ ). The patterns were recorded over  $2\theta$  range of 5–35° using scanning speed of 2° min<sup>-1</sup>. The crystalline index (%CI) was calculated with one replicate per sample according to Equation (1).

$$\%CI = \left( \frac{\sum A_{\text{crystalline}}}{A_{\text{total}}} \right) \times 100\%, \quad (1)$$

where  $\sum A_{\text{crystalline}}$  is the sum of areas under the crystalline peaks and  $A_{\text{total}}$  is the sum of areas under each peak. The areas were obtained by Gaussian deconvolution of the individual peaks using the software MagicPlot Student. The samples were stored at 25°C and 53% RH for 48 h prior to analysis.

## 2.4.3 | Fourier transform infrared spectroscopy

Fourier transform infrared spectroscopy (FTIR) spectroscopy was conducted at 25°C on a Bruker Vertex 50 spectrometer using the attenuated total reflectance (ATR) mode. The spectra were recorded from 4000 to 400 cm<sup>-1</sup> with 32 spectral accumulations and resolution of 4 cm<sup>-1</sup>. The measurements were performed with one replicate per sample (stored at 25°C and 53% RH for 48 h before analysis).

## 2.4.4 | Optical microscopy

Optical microscopy (OM) analysis was carried out with a BEL Solaris optical microscope. Film samples were mounted between two polycarbonate transparent laminas. The images were recorded in the bright-field mode using magnification of 4× (scale of 22 μm).

## 2.4.5 | Scanning electron microscopy

Scanning electron microscopy (SEM) was carried out on a JMS 6510 microscope (JEOL, Japan). Film samples

were cryo-fractured into liquid N<sub>2</sub> and covered with a thin gold layer for cross-sectional surface imaging. The SEM micrographs were taken using the secondary electron detector and an accelerating voltage of 5 kV.

## 2.4.6 | Mechanical tests

The films were subjected to tensile tests in a TA.XT.Plus Texturometer, with samples measuring 100 mm × 10 mm, distance between grips of 70 mm and stretching speed of 5 mm min<sup>-1</sup>. Relative humidity and temperature during the tests were kept constant at 56% and 25°C, respectively. The samples were stored at 25°C and 53% RH for 48 h prior to mechanical tests.

## 2.4.7 | Water contact angle measurements

Water contact angle (WCA) measurements were performed on a tensiometer CAM 101 (KSV Instruments, Finland) equipped with a CCD camera KGV-5000. The samples were mounted on an acrylic support, water droplets were carefully poured on their surface, and then drop images were taken automatically for 60 s. Contact angle values were calculated using the KSV CAM2008 software. Equations (2)–(4) were used to determine the interfacial energies<sup>24,25</sup>:

$$\cos \theta = \frac{\gamma_{\text{SV}} - \gamma_{\text{SL}}}{\gamma_{\text{LV}}}, \quad (2)$$

$$\cos \theta = \frac{(0.015\gamma_{\text{SV}} - 2)\sqrt{\gamma_{\text{LV}}\gamma_{\text{SV}}} + \gamma_{\text{LV}}}{\gamma_{\text{LV}}(0.0015\sqrt{\gamma_{\text{LV}}\gamma_{\text{SV}}} - 1)}, \quad (3)$$

$$\gamma_{\text{SL}} = \frac{\sqrt{\gamma_{\text{LV}}} - \sqrt{\gamma_{\text{SV}}}}{1 - 0.0015\sqrt{\gamma_{\text{LV}}\gamma_{\text{SV}}}}, \quad (4)$$

where  $\theta$  is the contact angle,  $\gamma_{\text{SV}}$  is the solid–vapor interfacial tension,  $\gamma_{\text{SL}}$  is the solid–liquid interfacial tension, and  $\gamma_{\text{LV}}$  is the liquid–vapor interfacial tension. The WCA measurements were performed in triplicate. The samples were stored at 25°C and 53% RH for 48 h before the analysis.

## 2.4.8 | WVP determinations

WVP tests were conducted in triplicate as per the classical gravimetric ASTM E96 standard. The WVP (g h<sup>-1</sup> m<sup>-1</sup> Pa<sup>-1</sup>) of the films was calculated by Equation (5):

$$\text{WVP} = \frac{\text{WVT} \times t}{P_s(R_1 - R_2)A}, \quad (5)$$

where WVT is the water vapor transmission rate ( $\text{g s}^{-1} \text{m}^{-2}$ ), determined as the slope of the mass loss (g) versus time (h) curve,  $A$  is the film permeation area ( $\text{m}^2$ ),  $P_s$  is water vapor saturation pressure at  $32^\circ\text{C}$  (98,066.5 Pa),  $R_1$  is the relative humidity inside the permeation cell filled with pure water (equal to 100%),  $R_2$  is the ambient relative humidity (equal to 51%), and  $t$  is the film thickness (m). The samples were stored at the same conditions prior to the WVP analysis— $25^\circ\text{C}$  and 53% RH for 48 h.

#### 2.4.9 | Determination of water uptake by immersion

Water uptakes were obtained by immersion of 0.1 g of film sample in 40 mL of deionized water. The samples were kept at minimum humidity for 72 h before being tested. After 24 h, a 4-mL aliquot ( $4 \times 1 \text{ mL}$ ) of the water in which the films were kept was taken and weighted, as well as pure deionized water. The mass difference between them was considered to be proportional to the total mass of water absorbed by the films, as shown in Equation 6. The water uptake was measured in milligrams of deionized water absorbed by grams of film for hour.

$$\text{Water uptake} = \frac{(m_{\text{initial}} - m_{\text{final}}) 1000 (m_{\text{water}}/m_{\text{initial}})}{m_{\text{sample}} t}, \quad (6)$$

where  $m_{\text{initial}}$  is the mass of aliquot of pure deionized water (m),  $m_{\text{final}}$  is the mass of the aliquot of the water where the films were kept (g), 1000 is a constant for conversion from grams to milligrams,  $m_{\text{water}}$  is the total mass of the water where the films were kept (g),  $m_{\text{sample}}$  is the mass of films added (g), and  $t$  is the analysis time (h). All the measurements were done in triplicate.

#### 2.4.10 | Life cycle assessment

Cradle-to-grave life cycle assessment (LCA) was conducted as per ISO 14040.<sup>26</sup> The product system boundary included CS, BW, and glycerol productions, film-forming solution preparation, CSC, and two possible end-of-life scenarios, namely, closed composting and municipal landfilling. All background LCI data for energy and material inputs were selected from the Product

Environmental Footprint (PEF) database, version 2.0. The functional unit was set to 1 ton of plastic film. The LCIA stage was implemented using the openLCA software (GreenDelta, Germany) and the PEF impact assessment method was applied to calculate the following midpoint eco-indicators: climate change (in  $\text{kg CO}_2 \text{ eq.}$ ), land use (in  $\text{m}^2 \text{ land}$ ), and water use (in  $\text{m}^3 \text{ H}_2\text{O}$ ).

#### 2.4.11 | Statistical analysis

Data were subjected to one-way analysis of variance (ANOVA) with the aid of the Past software. Mean values were compared using the Tukey's test at a confidence level of 95% ( $p < 0.05$ ).

## 3 | RESULTS AND DISCUSSION

### 3.1 | Starch/BW films produced by CSC

DSC was first carried out to simulate the thermal history of the starch/BW solutions throughout the continuous casting process. Typical DSC curves are shown for pure BW, pure starch (CS), and 10/5 and 10/7 starch/BW solutions in Figure 1d. For CS, it is observed a wide endothermic band ascribed to water evaporation in the heating zone I ( $T = 80^\circ\text{C}$ ), as expected. The second endothermic band relates to the elimination of residual water, indicating that the starch film is fully formed in the heating zone II ( $T = 120^\circ\text{C}$ ). The DSC curve of pure BW showed endothermic and exothermic peaks in the heating zone I and II, which are attributed to the melting and crystallization of BW components, respectively.<sup>27</sup> These processes are represented by a more prominent peak (related to BW ester components) and a shoulder (related to BW fatty acids).<sup>27</sup> For the 10/5BW and 10/7BW solutions, it is noticed an intermediate behavior with overlapped thermal events following the starch/BW ratio. The first endothermic band was significantly hastened at lower temperatures compared with CS due to the overall low  $T_m$  of BW, while the second endothermic band was determined by the  $T_m$  of BW fatty acid components. These results suggest the reversible phase change of BW in the presence of starch, also indicating that an immiscible system between starch and BW was formed. A second deduction is that the BW ester components crystallized to a lower extent possibly due to chemical interactions with the starch phase, as the corresponding crystallization peak was less pronounced in the DSC curves.

The CSC was performed at a moderately high temperature, drastically reducing the drying time of starch/BW solutions. The solutions containing 7 wt% starch

TABLE 2 Outcomes of bench solution casting methods applied to starch films modified with hydrophobic agents.

Starch source	Hydrophobic agent	Casting temperature	Productivity ( $\text{m}^2 \text{ film h}^{-1}$ )	Reference
Corn	Sunflower oil	60°C	0.0004	García et al. <sup>18</sup>
Corn	Soybean oil	25°C	0.0083	Bravin et al. <sup>28</sup>
Pea	Beeswax	25°C	0.0002	Han et al. <sup>19</sup>
Corn	Span 40, 60, and 80	20°C	0.0004	Ortega-Toro et al. <sup>29</sup>
Tapioca	Beeswax	25°C	0.0002	Pérez-Gallardo et al. <sup>16</sup>
Corn	Zein-rutin nanoparticles	45°C	0.0008	Zhang & Zhao <sup>30</sup>
Cassava	Beeswax	40°C	>0.0001	Pérez-Vergara et al. <sup>31</sup>
Corn	Beeswax	80–120°C	0.5500	This work

exhibited pseudoplastic behavior and high viscosity ( $\eta = 1.2 \text{ cP}$ ) (Figure S1), forming a stable wet layer onto the substrate moving at  $0.12 \text{ m min}^{-1}$  ( $\gamma = 1.5 \text{ s}^{-1}$ ).<sup>22</sup> As reported in Table 1, the film thickness was approximately  $50 \mu\text{m}$  for the various starch/BW ratios. More importantly, the productivity reached herein was  $0.55 \text{ m}^2 \text{ film min}^{-1}$ , which was at least 50-fold higher than those achieved for most bench cast starch films loaded with hydrophobic agents (Table 2). It is noteworthy that the CSC productivity can be further optimized, evidencing that the production of starch films loaded with BW can be leveraged to a large scale by CSC.

### 3.2 | Microstructural characterizations

ATR-FTIR analysis was conducted to indicate possible interactions between the starch and BW phases. Full band assignment is provided in Table S2. No significant differences were observed in the spectra, except for the bands at  $3300 \text{ cm}^{-1}$  (Figure 2a),  $2920\text{--}2890 \text{ cm}^{-1}$  (Figure 2b) and  $1730\text{--}1720 \text{ cm}^{-1}$  (Figure 2c) ascribed to O–H, C–H, and C=O stretching vibrations, respectively. Compared to the CS spectrum, the intensity of the OH band decreased, whereas the intensity of the C–H and C=O bands increased with increasing BW content in the films. In addition, a shift was observed in the carbonyl band (Figure 2c), comparing pure BW and starch/BW films. This suggests a possible interaction between OH groups of starch chains and COOH groups of BW monoesters and fatty acids.<sup>32</sup>

Bright-field optical microscopy (BF-OM) and scanning electron microscopy (SEM) were conducted to elucidate the morphology of the starch/BW films. BF-OM and SEM images are shown in Figure 3a–d and Figure 3e–h, respectively. It is possible to see that CS had a homogeneous and compact microstructure (Figure 3a,e). The dark dots seen in Figure 3a are related to defects resulting from the CSC process. The films incorporated with BW,

however, displayed a biphasic morphology, confirming the immiscibility between starch and BW. In Figure 3b, it is possible to observe the rounded BW domains embedded in the film structure tending to coalescence as the BW content increased (Figure 3c,d), forming heterogeneous lipidic domains, as previously reported by Han et al.<sup>19</sup> The SEM micrographs (Figure 3f–h) clearly revealed discrete micro-sized BW droplets distributed across the starch matrix rather than a bilayer structure that could result from a total phase separation and density difference between starch and BW. Pervaiz et al.<sup>33</sup> obtained thermoplastic starch (TPS) containing up to 10 wt% BW, but no phase identification was attained by SEM. The morphology of the 10/3BW, 10/5BW, and 10/7BW films may be explained by the fast drying of starch/BW solutions in the CSC process, which reduced the BW droplet coalescence to a considerable extent. It is worth pointing out that such a morphology was achieved without the use of any compatibilizer, as typically performed in starch/BW films. Additionally, no clear voids were observed at the starch/BW droplet interface, even for the highest BW content, despite the polarity difference between starch and BW. This indicates that the minimum hydrogen bonding formed between starch chains and BW ester compounds, as suggested by ATR-FTIR (Figure 2), was sufficient to promote a good interfacial adhesion in the starch/BW films.

The crystallinity of the continuously cast starch/BW films was assessed by XRD. The diffractograms of pure starch film (CS), pure BW (BW), and starch/BW films (10/3BW–10/7BW) are shown in Figure 4. CS showed no discernible reflections, indicating a complete starch gelatinization. The starch/BW films displayed reflections at  $2\theta = 19.6^\circ$ ,  $21.4^\circ$ , and  $23.8^\circ$  related to the fatty acid, hydrocarbon, and ester crystals, respectively, present in BW,<sup>10,14</sup> confirming the crystallization of BW during the CSC process.

XRD provided evidence that the BW phase accounted for the crystalline content of the starch/BW films

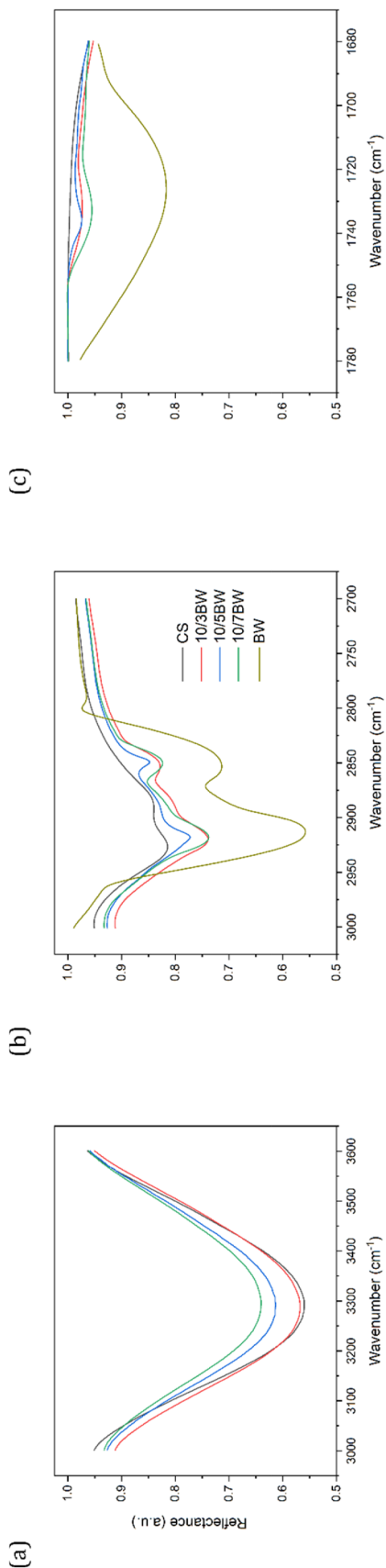


**FIGURE 2** ATR-FTIR spectra of pure starch film (CS), pure BW, and starch/BW films obtained by CSC. Selected spectral ranges of (a) 3600–3000  $\text{cm}^{-1}$ , (b) 3000–2700  $\text{cm}^{-1}$ , and (c) 1780–1680  $\text{cm}^{-1}$ . ATR, attenuated total reflectance; BW, beeswax; CS, corn starch; CSC, continuous solution casting; FTIR, Fourier transform infrared spectroscopy. [Color figure can be viewed at [wileyonlinelibrary.com](http://wileyonlinelibrary.com)]

obtained by CSC, as no reflections attributed to retrogradation of starch were observed in the diffractograms in Figure 4. Pure BW had a crystallinity index (%CI) equal to 65%, higher than that of CS (2.3%), and the %CI values of the starch/BW films increased with increasing the BW volumetric fraction (7.8% for 10/3BW and 16.9% for 10/7BW). However, these experimental values were lower than the theoretical %CI calculated by the rule of mixtures ( $\%CI_{\text{TOTAL}} = \phi_{\text{CS}} \%CI_{\text{CS}} + \phi_{\text{BW}} \%CI_{\text{BW}}$ ), suggesting that the BW crystallization was impaired (Table 3). This may be explained by the fast cooling and short drying time applied to the solutions in the CSC process, which possibly hindered the BW molecules to arrange into crystalline domains. In addition, the BW components may have interacted with the amylose and amylopectin chains (Figure 2), reducing their spatial ordering, thus reducing the crystallinity of the BW domains.

Overall, the films showed a homogeneous aspect to the naked eye; however, optical measurements revealed that the luminous transmittance significantly decreased from the control (CS) to the 10/7BW film (Table S1). Handling them without forming cracks was possible due to their mechanical integrity, even at the highest BW content (10/7BW).

Results of mechanical tensile tests are shown in Table 3 and in Figure 5. The addition of BW reduced the tensile strength of the starch films due to its inherently low mechanical properties. For the elastic modulus, the BW incorporation represented an increase in relation to the pure starch film (CS) for 10/3BW and 10/5BW formulations, suggesting that an interaction with wax components restricted the mobility of matrix chains, also causing the reduction of elongation at break. Auras et al.<sup>13</sup> incorporated BW into cassava starch films and found an increase in maximum elongation and a reduction in tensile strength and elastic modulus for increasing levels of BW. For the 10/7BW formulation, elastic modulus and elongation at break values were close to those of unmodified starch films. At  $\phi_{\text{BW}} = 0.46$ , a phase inversion occurred, since starch volumetric fraction was equal to 0.42, and the mechanical properties of the films were directly influenced by the BW properties. As BW is a soft material, a film composed mostly by this lipid shows a reduction in the elastic modulus and an increase in the elongation at break. However, such results could not be confirmed since the texturometer claws crushed the pure BW specimens due to their low stiffness, making any measurement of properties unfeasible.

### 3.3 | Moisture barrier properties

Table 4 shows the WVP results of the film samples. It is observed that the starch/BW films had drastically lower

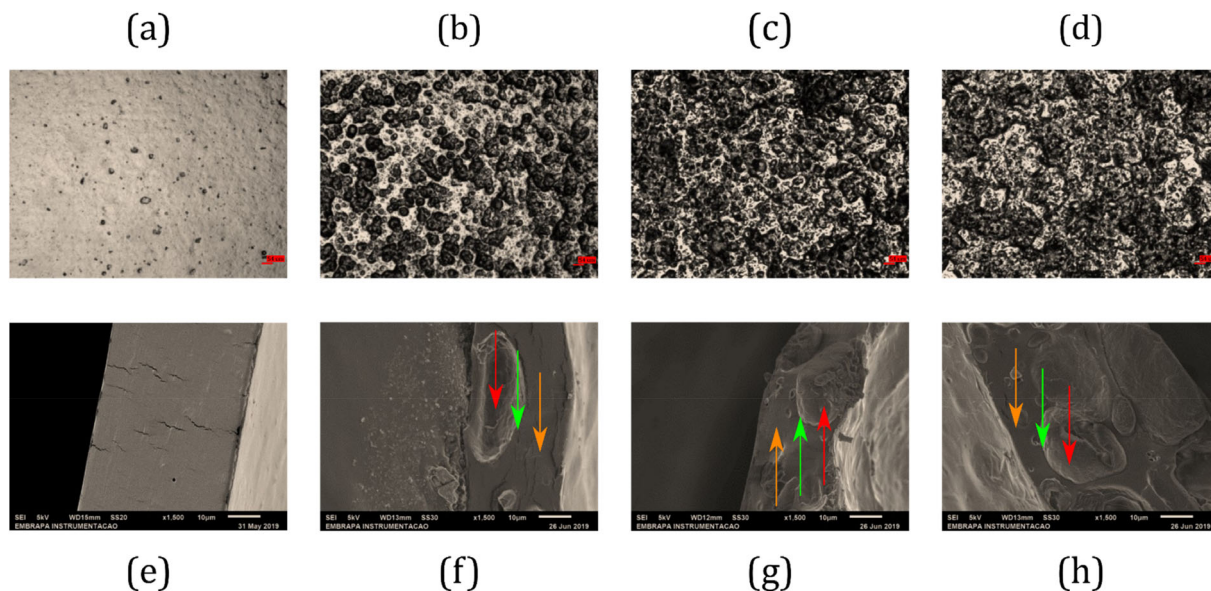


**FIGURE 3** Bright-field optical microscopy images of (a) CS, (b) 10/3BW, (c) 10/5BW, and (d) 10/7BW; black structures are beeswax (BW) domains dispersed in the corn starch (CS) matrix, in white. Scanning electron micrographs of (e) CS, (f) 10/3BW, (g) 10/5BW, and (h) 10/7BW films; arrows: red, BW droplets; orange, starch matrix; green, starch/BW interface. [Color figure can be viewed at [wileyonlinelibrary.com](http://wileyonlinelibrary.com)]

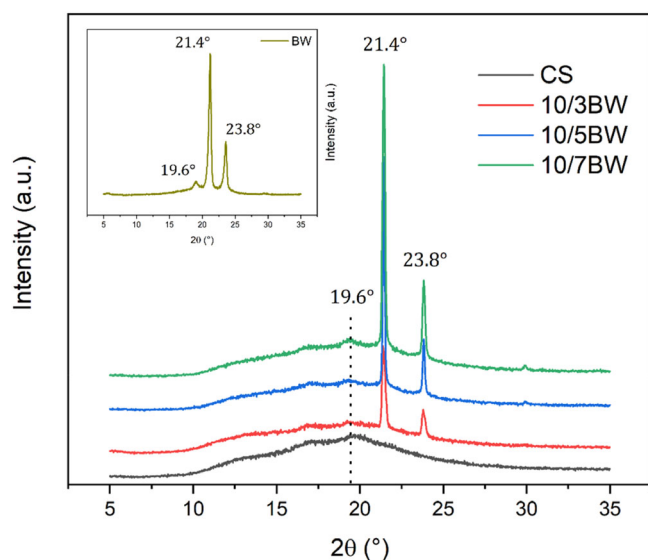


**FIGURE 4** X-ray diffractograms of pure starch film (CS) and starch/bee wax (BW) films obtained by continuous solution casting (CSC). The x-ray diffractogram of pure BW is depicted as an insert. CS, corn starch. [Color figure can be viewed at [wileyonlinelibrary.com](http://wileyonlinelibrary.com)]

WVP compared to CS ( $p < 0.05$ ), representing, for instance, the largest 0.8-fold reduction in WVP for a starch/BW mass ratio of 0.3 (10/3BW) ( $p < 0.05$ ). The reduced WVP of these continuously cast starch/BW films exceeded the previous WVP outcomes for bench cast starch films loaded with BW and other hydrophobic

compounds. For instance, Han et al.<sup>19</sup> found a 0.2-fold reduction in the WVP of pea starch films having BW contents larger than 30 wt%, indicating that the film still exhibited voids and channels enough to still allow H<sub>2</sub>O vapor diffusion. Oliveira et al.<sup>21</sup> and Ochoa et al.<sup>15</sup> observed a 0.5-fold reduction in the WVP of CS and oxidized starch films included with 5–10 wt% saponified sunflower-based and 0.2–1.0 wt% tween 80-based BW microemulsions, respectively. CS films loaded with sunflower oil (SO) exhibited a 0.5-fold reduction in WVP, which was attributed to the hydrophobic character of SO.<sup>18</sup> Pervaiz et al.<sup>33</sup> obtained thermoplastic corn starch (TPS) films with 5–10 wt% BW and paraffin wax by melt-extrusion (155–180°C), but no significant changes in water absorption were observed, being attributed to the loss of waxes in the process. Accordingly, the increase of hydrophobic fractions with higher crystallinity indexes (65% for BW, Table 3) and their stable and homogeneous microstructural distribution are key factors for increasing the moisture barrier properties of starch films. As observed in Figure 3, the semicrystalline BW droplets distributed within the starch matrix probably increased the tortuosity of the H<sub>2</sub>O vapor molecules diffusional pathway, thereby reducing the water vapor diffusion rate throughout the films. These comparisons denote the effectiveness of CSC in scaling up the production of starch/BW films using low temperatures to achieve superior water barrier properties.

The decreased WVP of the starch/BW films could also be due to the interference of BW droplets on the water



**TABLE 3** Beeswax (BW) mass fraction ( $\phi_{\text{BW}}$ ), measured and theoretical crystallinity index and mechanical properties (TS, tensile strength, EB, elongation at break, and YM, Young's modulus) of continuously cast starch/BW casting.

Sample	$\phi_{\text{BW}}$	Measured %CI	Theoretical %CI	TS (MPa)	EB (%)	YM (MPa)
CS	0.0	2.3	0	$2.11 \pm 0.94^{\text{a}}$	$58.43 \pm 1.44^{\text{a}}$	$16.96 \pm 1.69^{\text{a}}$
10/3BW	0.27	7.8	19.2	$1.99 \pm 0.04^{\text{a}}$	$21.23 \pm 0.67^{\text{a}}$	$87.33 \pm 1.69^{\text{a}}$
10/5BW	0.38	13.0	26.1	$1.52 \pm 0.05^{\text{a}}$	$22.33 \pm 0.94^{\text{a}}$	$81.38 \pm 1.08^{\text{a}}$
10/7BW	0.46	16.9	31.3	$0.94 \pm 0.04^{\text{a}}$	$67.82 \pm 2.83^{\text{a}}$	$14.78 \pm 0.60^{\text{a}}$

Abbreviation: CS, corn starch.

<sup>a</sup>Confidence level of statistical analysis was 95% ( $p < 0.05$ ).

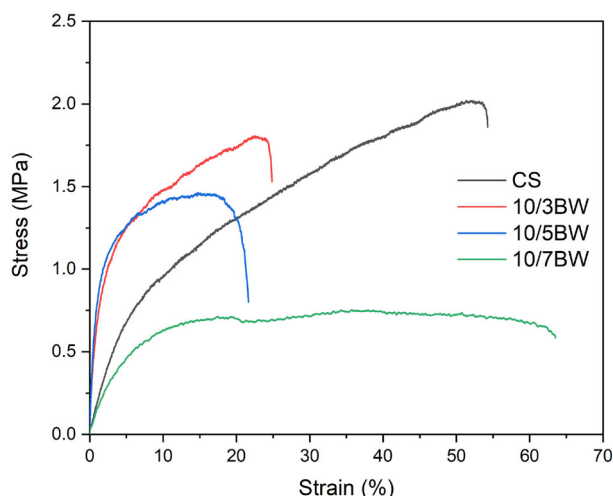


**FIGURE 5** Representative stress–strain curves of CS, 10/3BW, 10/5BW, and 10/7BW films obtained by tensile tests. BW, beeswax; CS, corn starch. [Color figure can be viewed at [wileyonlinelibrary.com](http://wileyonlinelibrary.com)]

vapor sorption process on the starch film surface. WCAs were determined for BW, CS and the ensuing starch/BW films, and the results are also listed in Table 4. It can be verified that the addition of BW doubled the contact angle of the starch matrix, making the films as hydrophobic as pure BW. This points out that the solid-vapor interfacial tension and surface free

energy of the starch films were reduced, that is, the kinetic energy of water vapor molecules exceeded the energy of attraction to the film surface, reducing the sorption rate.<sup>34</sup> The solid-vapor ( $\gamma_{\text{SV}}$ ) and solid-liquid ( $\gamma_{\text{SL}}$ ) surface tensions decreased with increasing the BW content, demonstrating the decreasing tendency to replace solid-vapor interfaces with solid-water ones (Table 4). This means that the addition of BW made the film surface wavier and more water-repellent,<sup>35</sup> blocking the overall permeation process, leading to low WVP values as the outcome.

Beyond that, water uptake is another factor that could be also associated with the decrease in WVP values, as shown in Table 4. The CS film kept 24 h immersed in deionized water absorbed five times more water than the starch/BW films. According to Hansen,<sup>36</sup> the solubility parameter of a polymer is the sum of dispersion, polar and hydrogen-bonding forces contributions. Dispersion forces are small compared to the other two and, therefore, can be neglected.<sup>36</sup> When BW is added, polar and hydrogen-bonding forces of the films are reduced because of the hydrophobic character of the wax. The former, due to the presence of non-polar chains in the BW composition; the latter, due to the intermolecular interaction between starch OH groups and BW COOH groups. Therefore, the interaction of the film matrices with water is directly impacted by the presence of BW.

**TABLE 4** Water contact angle (WCA), water vapor permeability (WVP), solid-vapor ( $\gamma_{\text{SV}}$ ) and solid-liquid ( $\gamma_{\text{SL}}$ ) surface tensions, and water uptake of pure beeswax (BW), pure starch film (CS) and starch/BW films (10/3BW, 10/5BW, and 10/7BW).

Sample	WVP ( $\text{g h}^{-1} \text{m}^{-1} \text{Pa}^{-1}$ )	$\gamma_{\text{SV}} = \gamma_{\text{s}}$ ( $\text{mN m}^{-1}$ )	$\gamma_{\text{SL}}$ ( $\text{mN m}^{-1}$ )	WCA	Water uptake ( $\text{mg g}^{-1} \text{h}^{-1}$ )
CS	$3.06 \pm 0.39^{\text{a}}$	$236.5 \pm 2.2^{\text{a}}$	$189.2 \pm 0.5^{\text{a}}$	$47.5 \pm 1.9^{\text{a}}$	$503 \pm 143^{\text{a}}$
10/3BW	$0.82 \pm 0.05^{\text{a}}$	$156.8 \pm 2.1^{\text{a}}$	$168.3 \pm 0.6^{\text{a}}$	$97.8 \pm 1.2^{\text{a}}$	$84 \pm 26^{\text{a}}$
10/5BW	$0.97 \pm 0.12^{\text{a}}$	$151.6 \pm 1.6^{\text{a}}$	$166.5 \pm 0.5^{\text{a}}$	$101.1 \pm 1.0^{\text{a}}$	$102 \pm 39^{\text{a}}$
10/7BW	$0.97 \pm 0.11^{\text{a}}$	$151.2 \pm 1.6^{\text{a}}$	$166.4 \pm 0.5^{\text{a}}$	$101.4 \pm 1.0^{\text{a}}$	$85 \pm 39^{\text{a}}$
Beeswax	-	$145.0 \pm 0.5^{\text{a}}$	$164.5 \pm 0.2^{\text{a}}$	$105.2 \pm 2.5^{\text{a}}$	-

Abbreviation: CS, corn starch.

<sup>a</sup>Confidence level of statistical analysis was 95% ( $p < 0.05$ ).

TABLE 5 Life-cycle assessment (LCA) results of continuously cast starch/beeswax (BW) films considering different end-of-life scenarios.

Sample	Closed composting			Municipal landfill		
	Climate change (kg CO <sub>2</sub> eq)	Land use (m <sup>2</sup> )	Water use (m <sup>3</sup> H <sub>2</sub> O)	Climate change (kg CO <sub>2</sub> eq)	Land use (m <sup>2</sup> )	Water use (m <sup>3</sup> H <sub>2</sub> O)
CS	35,877	151,158	19,561	36,886	151,123	19,549
10/3BW	29,200	128,381	15,940	30,212	128,346	15,927
10/5BW	25,986	117,414	14,196	26,998	117,379	14,184
10/7BW	23,415	108,640	12,801	24,427	108,605	12,789

Abbreviation: CS, corn starch.

### 3.4 | Eco-indicators of starch/BW films

Table 5 shows the results of the LCA from which three eco-indicators factors were analyzed and embrace many of the most important ones. The land and water use indicators are related to the area of land (m<sup>2</sup>) and volume of water (m<sup>3</sup>) demanded to produce and dispose a certain amount of film (1 metric ton, in the case of this work). The climate change indicator is related to the amount of greenhouse gases emitted during the production and disposal of the same quantity of film. It is notable that high contents of BW reduced the potential impacts concerning all eco-indicators. Moreover, two disposal methods (end-of-life scenarios) were compared. A greener closed composting method showed lower impacts on the environment than municipal landfilling, despite this difference being not so big. That was expected once the closed composting consists in the controlled degradation of the waste to reuse the gases emitted during the decomposition process. Consequently, the impact of this technique on the environment is less pronounced than the municipal landfill, which consists by simply discarding the films on the ground without any method to reuse the by-side residues of decomposition.

## 4 | CONCLUSIONS

CSC was proven to be a resourceful technique for producing hydrophobic starch/BW films intended as biodegradable plastics. Specifically, micro-sized BW droplets (at a minimal 30 wt%) well distributed throughout the starch matrix greatly reduced the surface hydrophilicity, water vapor diffusion and, consequently, maximized the moisture barrier properties of the starch/BW films. Such an emulsified film morphology was attained owing to the continuous casting approach that hastened the drying of solutions to further prevent the BW droplets from coalescence. The BW composition also aided the phase cohesiveness in the starch/BW films, as some of the less

hydrophobic BW components (short-chain esters, fatty acids, and alcohols) may have compatibilized the starch/BW interface. We expect that the starch/BW films and the continuous casting technique will serve as the basis for new developments of hydrophobic formulations able to step up biodegradable starch-based plastics toward viable food packaging, disposable bags, and other applications.

### AUTHOR CONTRIBUTIONS

**Bruno Ribeiro Luchesi:** Conceptualization (lead); data curation (lead); formal analysis (equal); investigation (lead); project administration (lead); writing – original draft (lead); writing – review and editing (equal). **Francys Kley Vieira Moreira:** Supervision (supporting); writing – review and editing (supporting). **José Manoel Marconcini:** Supervision (supporting); writing – review and editing (supporting).

### ACKNOWLEDGMENTS

The authors want to thank Conselho Nacional de Desenvolvimento Científico e Tecnológico – Brasil (CNPQ), Nanotechnology National Laboratory for Agriculture (LNNA), Embrapa Instrumentation and Federal University of São Carlos, Graduate Program in Materials Science and Engineering (PPGCEM–UFSCar). This study was financed in part by the Coordenação de Aperfeiçoamento de Pessoal de Nível Superior: 88887.388245/2019-00—Brasil (CAPES)—Finance code 001.

### DATA AVAILABILITY STATEMENT

The data collected in this work will be made available when requested.

### ORCID

Bruno Ribeiro Luchesi  <https://orcid.org/0000-0002-4589-4613>

### REFERENCES

- [1] A. Podshivalov, M. Zakharova, E. Glazacheva, M. Uspenskaya, *Carbohydr. Polym.* **2017**, *157*, 1162.

- [2] H. P. Nguyen Vu, N. Lumdubwong, *Carbohydr. Polym.* **2016**, *154*, 112.
- [3] A. de Campos, A. R. d. Sena Neto, V. B. Rodrigues, B. R. Luchesi, F. K. V. Moreira, A. C. Correa, L. H. C. Mattoso, J. M. Marconcini, *Carbohydr. Polym.* **2017**, *175*, 330.
- [4] Y. Wang, Q. Su, H. Wang, X. Zhao, S. Liang, *J. Appl. Polym. Sci.* **2019**, *136*, 136.
- [5] F. Xie, P. J. Halley, L. Avérous, *Progress in Polymer Science (Oxford)* **2012**, *37*, 595.
- [6] M. Schirmer, A. Höchstätter, M. Jekle, E. Arendt, T. Becker, *Food Hydrocolloids* **2013**, *32*, 52.
- [7] C. Bangyekan, D. Aht-Ong, K. Srikulkit, *Carbohydr. Polym.* **2006**, *63*, 61.
- [8] B. Ghanbarzadeh, H. Almasi, A. A. Entezami, *Innovative Food Sci. Emerging Technol.* **2010**, *11*, 697.
- [9] A. M. Slavutsky, M. A. Bertuzzi, *Food Packag Shelf Life* **2016**, *7*, 41.
- [10] Y. Gaillard, A. Mija, A. Burr, E. Darque-Ceretti, E. Felder, N. Sbirrazzuoli, *Thermochim. Acta* **2011**, *521*, 90.
- [11] A. P. M. Silva, A. V. Oliveira, S. M. A. Pontes, A. L. S. Pereira, M. d. s. M. Souza Filho, M. F. Rosa, H. M. C. Azeredo, *Carbohydr. Polym.* **2019**, *211*, 209.
- [12] A. P. Tulloch, *Chem. Phys. Lipids* **1971**, *6*, 235.
- [13] R. Auras, B. Arroyo, S. Selke, *Starch/Staerke* **2009**, *61*, 463.
- [14] A. A. Attama, B. C. Schicke, C. C. Müller-Goymann, *Eur. J. Pharm. Biopharm.* **2006**, *64*, 294.
- [15] T. A. Ochoa, B. E. García-Almendárez, A. A. Reyes, D. M. R. Pastrana, G. F. G. López, O. M. Belloso, C. R. González, *Food Bioprocess Technol.* **2017**, *10*, 103.
- [16] A. Pérez-Gallardo, B. García-Almendárez, G. Barbosa-Cánovas, D. Pimentel-González, L. R. Reyes-González, C. Regalado, *J. Food Sci. Technol.* **2015**, *52*, 5601.
- [17] C. B. Francisco, M. G. Pellá, O. A. Silva, K. F. Raimundo, J. Caetano, G. A. Linde, N. B. Colauto, D. C. Dragunski, *Int. J. Biol. Macromol.* **2020**, *152*, 272.
- [18] M. A. García, M. N. Martino, N. E. Zaritzky, *Food/Nahrung* **2001**, *45*, 267.
- [19] J. H. Han, G. H. Seo, I. M. Park, G. N. Kim, D. S. Lee, *J. Food Sci.* **2006**, *71*, 290.
- [20] A. Jiménez, M. J. Fabra, P. Talens, A. Chiralt, *Food Hydrocolloids* **2012**, *26*, 302.
- [21] V. R. L. Oliveira, F. K. G. Santos, R. H. L. Leite, E. M. M. Aroucha, K. N. O. Silva, *Food Chem.* **2018**, *259*, 55.
- [22] L. S. F. Leite, C. M. Ferreira, A. C. Corrêa, F. K. V. Moreira, L. H. C. Mattoso, *Carbohydr. Polym.* **2020**, *238*, 116198.
- [23] D. R. Munhoz, F. K. V. Moreira, J. D. Bresolin, M. P. Bernardo, C. P. De Sousa, L. H. C. Mattoso, *ACS Sustainable Chem. Eng.* **2018**, *6*, 9883.
- [24] D. Li, A. W. Neumann, *J. Colloid Interface Sci.* **1992**, *148*, 190.
- [25] W. A. Zisman, *Contact Angle, Wettability, and Adhesion*, ACS Publications, Washington **1964**, p. 1.
- [26] Associação Brasileira de Normas Técnicas, *ABNT NBR ISO 14040: Gestão ambiental-avaliação do ciclo de vida-princípio e estrutura*, ABNT, Rio de Janeiro **2009**.
- [27] R. Buchwald, M. D. Breed, A. R. Greenberg, *J. Exp. Biol.* **2008**, *211*, 121.
- [28] B. Bravin, D. Peressini, A. Sensidoni, *J. Food Eng.* **2006**, *76*, 280.
- [29] R. Ortega-Toro, A. Jiménez, P. Talens, A. Chiralt, *Food Hydrocolloids* **2014**, *38*, 66.
- [30] S. Zhang, H. Zhao, *Carbohydr. Polym.* **2017**, *169*, 385.
- [31] L. D. Pérez-Vergara, M. T. Cifuentes, A. P. Franco, C. E. Pérez-Cervera, R. D. Andrade-Pizarro, *NFS J.* **2020**, *21*, 39.
- [32] L. Svečnjak, G. Baranović, M. Vinceković, S. Prdun, D. Bubalo, I. T. Gajger, *J. Apic Sci* **2015**, *59*, 37.
- [33] M. Pervaiz, P. Oakley, M. Sain, *Int. J. Compos. Mater.* **2014**, *4*, 204.
- [34] S. T. Oyama, M. Yamada, T. Sugawara, A. Takagaki, R. Kikuchi, *J. Jpn. Pet. Inst.* **2011**, *54*, 298.
- [35] D. K. Owens, R. C. Wendt, *J. Appl. Polym. Sci.* **1969**, *13*, 1741.
- [36] C. M. Hansen, *I&EC Prod. Res. Dev.* **1969**, *8*, 2.

## SUPPORTING INFORMATION

Additional supporting information can be found online in the Supporting Information section at the end of this article.

**How to cite this article:** B. R. Luchesi, F. K. V. Moreira, J. M. Marconcini, *J. Appl. Polym. Sci.* **2023**, e54730. <https://doi.org/10.1002/app.54730>